

Granularity and Inhomogeneity Are the Joint Generators of Optical Rogue Waves

F. T. Arecchi,^{1,2} U. Bortolozzo,³ A. Montina,⁴ and S. Residori³

¹*Dipartimento di Fisica, Università di Firenze, Via Sansone 1, 50019 Sesto Fiorentino, Firenze Italy*

²*CNR-INO, largo Enrico Fermi 6, 50125 Firenze, Italy*

³*INLN, Université de Nice Sophia-Antipolis, CNRS, 1361 route des Lucioles, 06560 Valbonne, France*

⁴*Perimeter Institute for Theoretical Physics, Waterloo, Ontario, N2L 2Y5 Canada*

(Received 6 December 2010; revised manuscript received 8 March 2011; published 15 April 2011)

In the presence of many waves, giant events can occur with a probability higher than expected for random dynamics. By studying linear light propagation in a glass fiber, we show that optical rogue waves originate from two key ingredients: granularity, or a minimal size of the light speckles at the fiber exit, and inhomogeneity, that is, speckles clustering into separate domains with different average intensities. These two features characterize also rogue waves in nonlinear systems; thus, nonlinearity just plays the role of bringing forth the two ingredients of granularity and inhomogeneity.

DOI: [10.1103/PhysRevLett.106.153901](https://doi.org/10.1103/PhysRevLett.106.153901)

PACS numbers: 42.25.Dd, 05.45.-a, 42.65.Sf, 42.70.Df

Understanding the origin of the giant events appearing in systems characterized by many waves is currently a matter of debate [1]. Extreme waves, known as freak or rogue waves, appear spontaneously on the ocean surface and are a threat even to large ships and ocean liners. Several efforts have been made to explain ocean rogue waves and different mechanisms have been proposed, including focusing of line currents [2], nonlinear focusing via modulational instability [3], and breather collision [4]. Most of the models, however, rely on a weakly nonlinear description of the interacting waves, based on the nonlinear Schrödinger equation, so that they fail, in general, to catch the very steep profile that characterizes the extreme events. In this context, numerical simulations play an important role shedding light on basically involved mechanisms, such as the role of large breathers [5], the Benjamin-Feir instability [6], and the emergence of extreme events from wave turbulence [7]. Recently, large scale experiments have been performed to study directional ocean waves [8], and the steadily growing interest in the subject has led to setup laboratory experiments dealing with rogue waves in such different systems as nonlinear light propagation in doped fibers [9,10], acoustic turbulence [11], nonlinear optical cavities [12], and microwave transport [13]. Despite the specificity of each experiment, a common feature shared by all the systems is the non-Gaussian statistics of the wave amplitude, with long tails of the probability density function (PDF) accounting for the rather frequent emission of the giant waves. Another common property is the existence of many uncorrelated grains inhomogeneously distributed in larger spatial domains. Depending on the system under study and on the nature of the waves considered, grains can be of a different origin, such as solitons in nonlinear systems [14] or wave packets in linear propagating waves, and their clustering in spatial domains can occur via different mechanisms, as, for instance, a temporal delay, a spatial symmetry breaking,

a transport phenomenon, or a hypercycle type amplification [15]. On the other hand, it has been recently outlined in the microwave experiment that rogue waves can occur even in the absence of nonlinearity [13].

Motivated by the existence of many strong similarities among different systems, and by the question of whether nonlinearity plays or not a fundamental role for the occurrence of rogue waves, we inquire whether there are key ingredients that provide rogue waves, and whether optical rogue waves need a nonlinear dynamics or can be observed even in a linear system, once those ingredients are present. For the sake of clarifying these issues, we have set up a linear optical experiment that demonstrates the two key elements that provide rogue waves, namely, granularity, that is, fragmentation of the wave field into a large number of elementary objects of still finite size (let us call them speckles), and inhomogeneity, that is, clustering of speckles in spatial domains with different average intensities. To transform this inhomogeneity into anomalous statistics, the detection process should be confined within a domain and then the different domains should be explored at separate times, either by moving the observer or jumbling the area observed by a fixed detector via some time dependent coupling. In the linear case, jumbling is due to a change of the optical paths toward the detector, driven by a suitable perturbation. In the nonlinear case [12], it is due to an alternation of the local excitations in presence of spatio-temporal chaos.

The experimental setup [Fig. 1(a)] consists of a multi-mode glass optical fiber (0.4 mm diameter and 2 m length) in which a laser beam is let to propagate. The input beam comes from a frequency doubled solid state laser, wavelength 532 nm. Less than 1 mW/cm² is coupled inside the fiber and the input profile is controlled by a spatial-light-modulator (SLM). This is a computer driven liquid crystal display, 768 × 1024 pixels, 1 in. diagonal size. By setting onto the SLM appropriate transmittance masks $T(x, y)$,

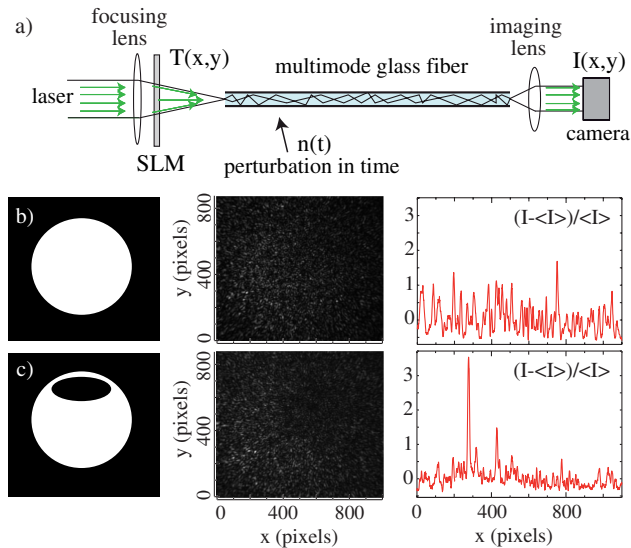


FIG. 1 (color online). (a) Experimental setup for the linear excitation of optical rogue waves: a laser input beam is focused and coupled into a multimode optical fiber; the output field is imaged onto a CCD camera; a SLM controls the input beam profile through variable transmittance masks $T(x, y)$; a lateral perturbation $n(t)$ rules the fiber bending. (b) Uniform and (c) inhomogeneous mask $T(x, y)$ (left), with corresponding output intensity distribution $I(x, y)$ (center) and one-dimensional intensity profile $I(x)$ (right) taken along an x line of the corresponding central image; I is the local intensity, and $\langle I \rangle$ is the intensity averaged over the whole image. An optical rogue wave can be clearly observed in the one-dimensional profile of case (c).

arbitrary profiles of the input intensity distribution can be introduced. A uniform mask and an inhomogeneous mask are depicted in the left panels of Figs. 1(b) and 1(c), respectively. While the uniform $T(x, y)$ allows the whole cone of input wave vectors to be coupled into the fiber, the black hole on the inhomogeneous $T(x, y)$ prevents the wave vectors passing in that direction to be coupled into the fiber, thus inducing at the output domains of different average intensity. In the central panels of Figs. 1(b) and 1(c) are shown the output intensity distributions $I(x, y)$ for the homogeneous and inhomogeneous mask, respectively. In the left panels of Figs. 1(b) and 1(c), one-dimensional intensity profiles taken along an x line of the corresponding images are displayed. In the inhomogeneous case, a large amplitude peak, or optical rogue wave, can be clearly distinguished.

In this setup the two joint generators of optical rogue waves, granularity and inhomogeneity, are simultaneously present. Granularity is a consequence of the interference among the many modes traveling down the fiber at different angles with respect to the axis, providing at the output a specklelike pattern composed of many spatial grains. The average size of the grains (single speckle) is given by the effective aperture of the fiber, the total number of modes supported by the fiber being proportional to $(a/\lambda)^2$, with a the radius of the fiber core and λ the wavelength of light in

air [16]. On the other hand, the inhomogeneous mask induces at the exit of the fiber an inhomogeneous distribution of the average intensity when it is evaluated over domains of adjacent grains.

In order to characterize the statistical properties of the output field we have recorded the PDF of the intensity under different experimental conditions. By acquiring with a CCD camera (768×1024 pixels and 12 bits depth) a large set of images (about 1000) and then performing the histograms of the intensity values on the whole image stack, we determine the PDF. The results are shown in Fig. 2(a), where the PDF recorded for a uniform $T(x, y)$ is compared with the PDF recorded in the presence of an inhomogeneous mask. The first one [gray (red) solid line] is well fitted by an exponential function (black dashed line), as expected for speckles [16]. The second one (empty black dots) shows appreciable, though not too large, deviations from the exponential. In the same figure we plot also a PDF with strong deviations from the exponential; it is obtained by applying to the fiber the lateral perturbation $n(t)$. For this purpose, a piezoelectric emitter has been placed in contact with a side of the fiber [see Fig. 1(a)]. Thanks to the elasto-optical effect, when the piezo emits a low frequency acoustic wave, it locally modifies the optical paths inside the fiber, giving rise to different spatial distributions of the output intensity; therefore, the detector collects events over different speckle configurations. The effect of the temporal modulation greatly enhances the stretched exponential character of the PDF of the intensity. Note, however, that in the inhomogeneous case the PDF is a stretched exponential even without temporal perturbations (even though small-tailed when compared to the perturbed case), while in the homogeneous case the PDF remains exponential even in the presence of temporal modulations. For comparison with other systems, for instance, with water waves where the wave height is taken from crest to trough, we plot in Fig. 2(b) the statistics of the local maxima of the intensity. As in water waves [8], we observe that the appearance of rogue waves is accompanied by a large increase of the skewness and kurtosis of the wave amplitude distribution.

When inhomogeneity and temporal perturbations are simultaneously present, the resulting large-tailed PDF of the intensity is well described by a stretched exponential distribution, that is (besides a normalization constant), $P(I) = e^{-\sqrt{c_1+c_2}I}$, where c_2 is a scale factor and c_1 a form parameter. In the limit $c_1 \rightarrow \infty$, the stretched distribution becomes an exponential. To account for the stretched exponential character of the PDF, let us consider the role of inhomogeneity. At the fiber exit the intensity is distributed as a collection of speckle patterns made of various domains with different average intensities. Within a single domain the statistics are exponential but the variance changes from domain to domain. As a consequence, the overall PDF becomes a stretched exponential

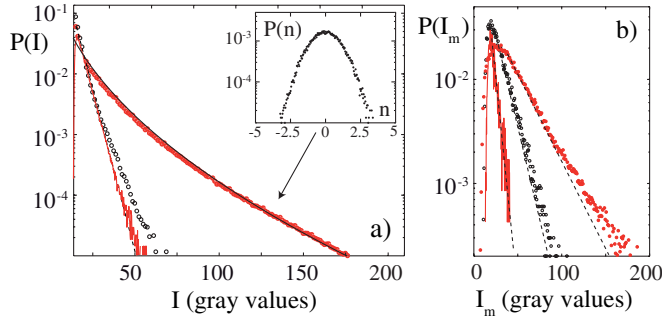


FIG. 2 (color online). PDF of (a) the intensity and (b) the local maxima of the intensity at the output of the fiber. Solid gray (red) line, homogeneous mask; (black) empty dots, inhomogeneous mask; (red) filled dots, inhomogeneous mask and temporal perturbations; black dashed line, fit with an exponential function. In (a) the black solid line is a stretched exponential fit ($c_1 = 10$, $c_2 = 0.092$) and the inset shows the Gaussian PDF of the perturbation $n(t)$ producing the large-tailed PDF. The intensities are measured in gray values normalized from 0 to 256 and all plots are in log-lin scale.

as the events are counted over the whole field. Similar results have been found in the microwave experiment [13]. More precisely, the stretched distribution can be obtained as a statistical mixture of many exponential distributions with different variances,

$$P(I) = \int_0^\infty d\sigma \rho(\sigma) \frac{e^{-I/\sigma}}{\sigma}, \quad (1)$$

where σ is the variance of the PDF in a single domain. The stretched distribution is exactly obtained when the distribution of σ is

$$\rho(\sigma) = \sqrt{\sigma} e^{-(c_2\sigma/4) - (c_1/2\sigma)}. \quad (2)$$

To evaluate the distribution of σ from the experiment we have subdivided each image of the output intensity in many domains of equal size, each containing only a few speckle grains, and we have evaluated the PDF on each single domain. The resulting PDF of the single domain is exponential, with a variance that changes from one domain to another. The resulting distribution of the measured variance is plotted in Fig. 3(a). Numerically, we have calculated the stretching parameter $1/c_1$ as a function of the tilt at the entrance of the fiber. The results, plotted in Fig. 3(b), confirm the essential role of inhomogeneity in enhancing the deviation from the exponential.

We consider, now, the statistics of the waiting times between successive rogue waves occurring at a given space position. As we limit our observations to a single homogeneous domain, we classify a Poisson distribution of event separation. However, as $n(t)$ jumbles the different domains within the detector aperture, we expect different rates associated with different domains. Interpolation of the different Poissonians should yield log-Poisson statistics for the waiting times between two successive events [17].

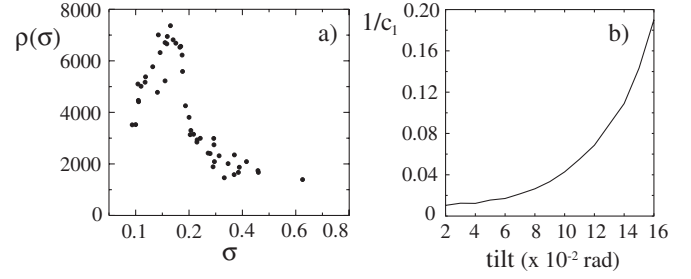


FIG. 3. (a) Experimental distribution of the variance σ of the single PDF measured over each homogeneous domain at the output of the optical fiber; (b) numerically calculated $1/c_1$ as a function of the tilt at the entrance of the fiber.

In the experiment, the events are recorded by placing a photodiode in a fixed point and by counting a rogue wave each time the intensity is above a given threshold, here taken as 4 times the average intensity. The waiting times are defined as $w = \ln(t_k) - \ln(t_{k-1}) = \ln(t_k/t_{k-1})$, where t_k is the occurrence time of the k th event. By analyzing the recorded data we obtain a log-Poisson distribution of the waiting time between successive events, as depicted in Fig. 4.

From the above results and considerations, we see that granularity and spatial inhomogeneity are joint generators that induce rogue waves even without nonlinearity. Nevertheless, the temporal scrambling of the spatially uncorrelated domains largely amplifies the deviations from the exponential statistics. We can, therefore, expect that in a nonlinear system where a spatiotemporal dynamics takes place spontaneously, the rogue wave phenomenon is very likely to be activated whenever clustering of grains occurs in inhomogeneous domains. In this perspective, it is useful to draw a comparison with a nonlinear case and we, therefore, refer to the optical experiment reported in Ref. [12], which consists of an unidirectional optical resonator where a nonlinear medium is pumped by an external beam and provides gain [18,19]. There, the nonlinearity yields transverse spatial grains whose average size is $(\lambda L)/a$, where L is the free propagation length in the optical cavity and a is the size of the most limiting aperture in the cavity [12].

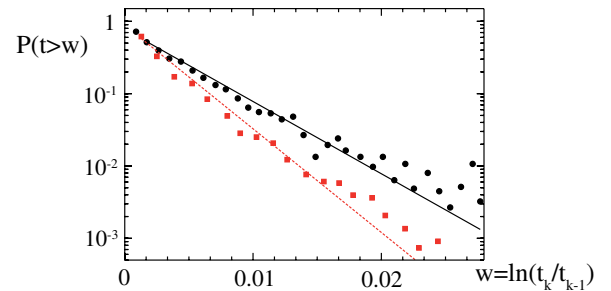


FIG. 4 (color online). Log-Poisson distribution of the waiting times between successive rogue waves; (red) squares and (black) dots correspond to, respectively, low and high amplitudes of $n(t)$.

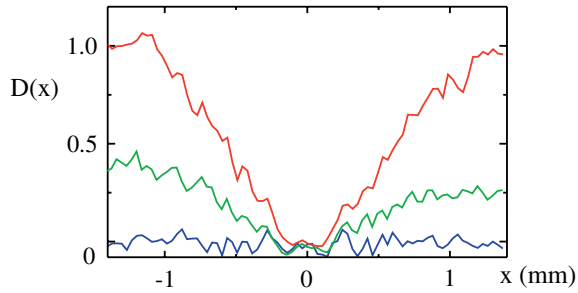


FIG. 5 (color online). Numerically calculated nondimensional indicator of rogue wave statistics for a nonlinear optical cavity vs the transverse coordinate x and for increasing pump intensity; $I_p/I_{th} = 4, 6, 8$ for the blue (lower), green (middle), and red (higher) curve.

The same scaling of the grain size was previously obtained for a photorefractive cavity characterized by a space-time chaotic behavior [20]. Inhomogeneity is then introduced by the chosen geometrical configuration of the resonator: if the coordinate system is taken such that z is along the cavity axis and x, y are on the transverse plane, there is an inversion symmetry around the y axis, which provides a nonlocal coupling between distant domains.

For relatively low intensity of the pump beam the cavity field shows a complex spatiotemporal dynamics. At higher pump intensity rogue waves appear as large amplitude peaks, and the PDF of the intensity becomes a stretched exponential, with c_2/c_1 increasing with the pump intensity [12]. As an indicator of the deviation from the exponential statistics we define here the nondimensional parameter $D(\vec{r}) = \langle I^2(\vec{r}) \rangle / \langle I(\vec{r}) \rangle^2 - 2$, which is equal to zero for exponential statistics and increases as c_1 decreases. In Fig. 5 we plot the numerically calculated $D(x)$, which is $D(\vec{r})$ integrated along the vertical axis, as a function of the horizontal transverse coordinate x and for $I_p/I_{th} = 4, 6, 8$, where I_p is the pump intensity and I_{th} the threshold intensity for the oscillation to start. We can see that $D(x)$ is an increasing function of both I_p and $|x|$. While for increasing I_p the increasing nonlinearity enhances the granularity, moving away from $x = 0$ (that is, the inversion symmetry axis of the system), the inhomogeneity increases. We can, therefore, conclude that granularity and inhomogeneity characterize rogue waves also in the nonlinear case. Nonlinearity has the role of bringing forth these two ingredients.

In conclusion, based on a linear experiment we have shown that granularity and spatial inhomogeneity are the two key ingredients for the occurrence of optical rogue waves. The evidence of rogue waves is represented by stretched exponential intensity statistics and by an associated log-Poisson distribution of occurrence times.

Furthermore, we have revisited some aspects of a previous nonlinear optical experiment [12], showing that the same considerations hold with a reinterpretation of inhomogeneity (that in Ref. [12] was arising from a transverse shift in the return light due to the cavity configuration), and of timing of data collection, that in the linear case is ruled by the fiber perturbation $n(t)$, whereas in the nonlinear case [12] it was intrinsic of the complex space-time dynamics, in the same way as granularity was spontaneously brought forth by nonlinearity. We expect the arguments provided here to hold in general for other wave systems, thus opening the way to a unified explanation of the rogue wave phenomenon.

Research at Perimeter Institute for Theoretical Physics is supported in part by the Government of Canada through NSERC and by the Province of Ontario through MRI.

-
- [1] N. Akhmediev and E. Pelinovsky, *Eur. Phys. J. Special Topics* **185**, 1 (2010), and articles therein.
 - [2] B. S. White, *J. Fluid Mech.* **355**, 113 (1998).
 - [3] M. Onorato, A. R. Osborne, and M. Serio, *Phys. Rev. Lett.* **96**, 014503 (2006).
 - [4] N. Akhmediev, J. M. Soto-Crespo, and A. Ankiewicz, *Phys. Lett. A* **373**, 2137 (2009).
 - [5] A. I. Dyachenko and V. E. Zakharov, *Pis'ma Zh. Eksp. Teor. Fiz.* **88**, 356 (2008).
 - [6] B. Eliasson and P. K. Shukla, *Phys. Rev. Lett.* **105**, 014501 (2010).
 - [7] K. Hammani, B. Kibler, C. Finot, and A. Picozzi, *Phys. Lett. A* **374**, 3585 (2010).
 - [8] M. Onorato *et al.*, *Phys. Rev. Lett.* **102**, 114502 (2009).
 - [9] D. R. Solli *et al.*, *Nature (London)* **450**, 1054 (2007).
 - [10] J. M. Dudley, G. Genty, and B. Eggleton, *Opt. Express* **16**, 3644 (2008).
 - [11] A. N. Ganshin *et al.*, *Phys. Rev. Lett.* **101**, 065303 (2008).
 - [12] A. Montina *et al.*, *Phys. Rev. Lett.* **103**, 173901 (2009).
 - [13] R. Hohmann *et al.*, *Phys. Rev. Lett.* **104**, 093901 (2010).
 - [14] N. Akhmediev and A. Ankiewicz, *Dissipative Solitons* (Springer, Berlin, 2005).
 - [15] M. Eigen and P. Schuster, *The Hypercycle: A Principle of Natural Self-Organization* (Springer, Berlin, 1979).
 - [16] J. W. Goodman, *Speckle Phenomena in Optics: Theory and Applications* (Roberts and Company Publishers, Greenwood Village, CO, 2007).
 - [17] Logarithmic waiting times typically occur in cooperative and complex systems. See, e.g., P. Sibani and P. B. Littlewood, *Phys. Rev. Lett.* **71**, 1482 (1993); T. O. Richardson *et al.*, *PLoS ONE* **5**, e9621 (2010).
 - [18] U. Bortolozzo *et al.*, *Phys. Rev. Lett.* **99**, 023901 (2007).
 - [19] U. Bortolozzo, S. Residori, and J. P. Huignard, *J. Phys. D* **41**, 224007 (2008).
 - [20] F. T. Arecchi *et al.*, *Phys. Rev. Lett.* **65**, 2531 (1990); **67**, 3749 (1991).